Total fusion cross section for the $^{16}O + ^{16}O$ system

I. Tserruya, Y. Eisen,* D. Pelte,† and A. Gavron
Department of Nuclear Physics, The Weizmann Institute of Science, Rehovot, Israel

H. Oeschler,‡ D. Berndt, and H. L. Harney
Max-Planck-Institut fur Kernphysik, Heidelberg, West Germany

(Received 1 February 1978)

Total fusion cross sections σ_F have been measured for $^{16}O + ^{16}O$ at bombarding energies 27–66 MeV using the E-ΔE or the time-of-flight techniques. The fusion excitation function shows oscillations in agreement with the resonances produced in the total reaction cross section by a surface-transparent potential. The results are compared to those obtained via the γ-ray technique and the importance of direct decay to ground states is discussed. Mass and total angular distributions are well reproduced by statistical model calculations which take angular momentum into account explicitly. Barrier and critical parameters are extracted from the average energy behavior of σ_F. No evidence for shell effects as predicted by Glas and Mosel is found on the measured fusion cross sections.

[NUCLEAR REACTIONS Complete fusion, $^{16}O + ^{16}O$, $E_{lab} = 27$–66 MeV; measured fusion excitation function; statistical model analysis; extracted barrier and critical parameters.]

I. INTRODUCTION

The study of heavy ion fusion cross sections has attracted considerable interest in the last years.[1] Essentially, such data allow the extraction of information about the nucleus-nucleus potential. At low incident energies close to the Coulomb barrier, the parameters R_B and V_B (the location and height of the interaction barrier) can be obtained.[2,3] At higher energies, the fusion data fix one value of the potential at a very close distance through the critical parameters R_C and V_C (Ref. 4) (assuming that fusion takes place whenever the colliding nuclei reach the distance R_C). The fusion cross section between nuclei in the $1p$ shell is of particular interest.[1] Large qualitative differences have been recently observed in the fusion data between systems which differ only by a few mass units. The most striking one is the observation of oscillations or resonances[5–8] in the excitation function of fusion between "α nuclei" such as $^{12}C + ^{12}C$, whereas neighboring systems such as $^{14}N + ^{12}C$ (Refs. 9 and 10) show the expected smooth behavior. Another anomaly appears in the maximum value σ_F^{max} of the fusion cross section. All investigated systems in the $1p$ shell have a nearly common value of $\sigma_F^{max} \approx 1000$ mb, with the exception of the $^{15}N + ^{12}C$ system which has the value $\sigma_F^{max} \approx 1150$ mb.[9] This larger value is close to the value of 1200 mb, which seems to be characteristic of systems involving one of the colliding nuclei in the sd shell.[11]

In addition to the above considerations, the $^{16}O + ^{16}O$ as a doubly closed-shell system presents other interesting features. For such a strongly bound system, Glas and Mosel have predicted a shell effect on the fusion data which should manifest itself in a smaller value of R_C compared to neighboring systems.[4,12] A comparison with other systems in this mass region can provide information on the role played by individual nucleons in the fusion process.

In this work we measured the $^{16}O + ^{16}O$ total fusion cross section σ_F in the energy range $E_{lab} = 27$–66 MeV. The evaporation residues have been directly detected using the ΔE-E or the time-of-flight technique.

An excitation function of the fusion cross section for the $^{16}O + ^{16}O$ system has been recently published by Kolata *et al.*[7] Before the completion of this work a similar study by Cheng *et al.*[13] became available. Both studies were carried out using the γ-ray technique. Their results will be compared to those obtained in the present study and the different measuring techniques will be discussed.

Section II describes the experimental method and shows the results. Section III presents the analysis and the discussion of the results, following the above-mentioned points. Evaporation calculations which take into account angular momentum are presented. A summary is given in Sec. IV.

II. EXPERIMENTAL PROCEDURE AND RESULTS

The $^{16}O + ^{16}O$ fusion excitation function has been measured in the energy range $E_{lab} = 27$–57 MeV in steps of 1 MeV and from 57 to 66 MeV in steps of 1.5 MeV. The measurements were carried out at the Weizmann Institute of Science using the ^{16}O

beams of the tandem EN accelerator (for the energy range $E_{lab} = 27-42$ MeV) and of the 14 UD Pelletron accelerator (for $E_{lab} = 45-66$ MeV). The experimental arrangement was similar to the one described in Ref. 14. Evaporation residues were detected using the ΔE-E technique, the ΔE being an ionization chamber of the type described by Fowler and Jared.[15] The telescope was operated at pressures of 15–25 Torr using a gas mixture of 90% Argon and 10% methane. Self-supporting NiO targets were used. The targets were prepared by oxidation of a 60 $\mu g/cm^2$ Ni foil of natural isotopic composition. Additional measurements from 45–66 MeV in steps of 3 MeV were performed with the ^{16}O beam of the tandem MP accelerator of the Max-Planck-Institut für Kernphysik at Heidelberg. In these runs the evaporation residues were detected with the time-of-flight (TOF) technique[16] and the targets consisted of self-supporting SiO_2 with a thickness of 50 $\mu g/cm^2$.

At low incident energies ($E \leq 36$ MeV), the kinetic energy of the evaporation residues is close to or below the Bragg maximum and the different elements cannot be resolved with the ΔE-E technique. But the total yield of evaporation residues was clearly and unambiguously identified. Figure 1 shows a two-dimensional display of $(E$-$\Delta E)$ vs ΔE taken at $E = 45$ MeV and at $\theta = 15°$. The different elements are quite well separated at this energy, and only a small fraction of the yield merges into the common Bragg curve. At higher energies this fraction becomes even smaller and the separation is better. Particles which were stopped in the ΔE counter or which did not reach the E counter due to multiple scattering in the entrance window and in the gas were also recorded and are displayed in the lowest $(E$-$\Delta E)$ channel in Fig. 1. These events were also considered evaporation residues when located below the whole group of fusion yield. This addition was generally small and amounted to less than 3% of the total fusion events.

Figure 2 shows a two-dimensional display of energy vs mass measured at $E = 60$ MeV with the TOF technique. The fusion products from $^{16}O + ^{16}O$ were clearly separated from those of $^{16}O + ^{28}Si$ and the different masses could be resolved in the group of evaporation residues from $^{16}O + ^{16}O$.

The vicinity of the target holder was cooled to dry ice temperature to minimize carbon buildup. Since a small amount of carbon buildup was still noticeable, the targets were changed after several hours of bombardment (typically 6–8 hours) so that the relative amount of carbon was below $\approx 4\%$.

At incident energies of $E \gtrsim 54$ MeV, the ^{16}O and Ni fuse with an appreciable cross section. Due to their very low kinetic energy the fusion products

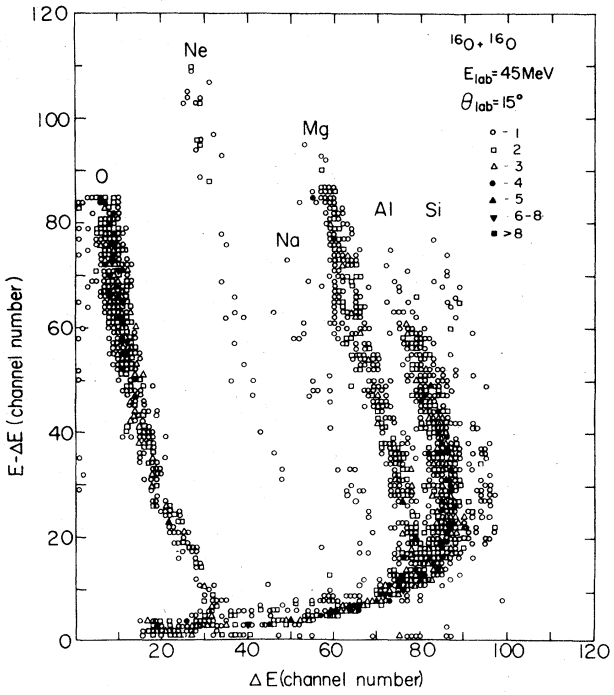

FIG. 1. $(E$-$\Delta E)$ vs ΔE spectrum for $^{16}O + ^{16}O$ taken at $E_{lab} = 45$ MeV and $\theta_{lab} = 15°$. The yield intensity is indicated in the figure. The high energy part of the O line is not presented.

interfere with those of $^{16}O + ^{16}O$ and it was necessary to correct the $^{16}O + ^{16}O$ fusion yield by subtracting the Ni contribution. This contribution was obtained from separate measurements of the ^{16}O + Ni fusion with a nonoxidized Ni foil of the same thickness (60 $\mu g/cm^2$) and using the elastic scattering peak of ^{16}O on Ni in the monitor counters (see below) for normalization. The relative magnitude of the correction increased with increasing bombarding energy and decreasing angle. It was generally small (~ 10%) and reached a maximum value of 25% at 66 MeV. The uncertainty of this correction was estimated to be less than 10%, thus producing a maximum error of 2.5% in σ_F.

In the $^{16}O + ^{16}O$ system there is some difficulty in separating the evaporation residues from direct reaction products. In Figs. 1 and 2 it is seen that the yield of $A = 17-19$ or $Z = 9$ is very low and the problem remains mainly in the case of ^{20}Ne where the α transfer and the 3α evaporation yields cannot be separated. The population of the g.s. and the two first excited states in ^{20}Ne (which appear as sharp lines in the ^{20}Ne spectrum) was attributed to the direct process. All other events of ^{20}Ne (which form a broad and continuous spectrum) and all products with $Z > 10$ or $A > 20$ were considered as evaporation residues and defined the fusion

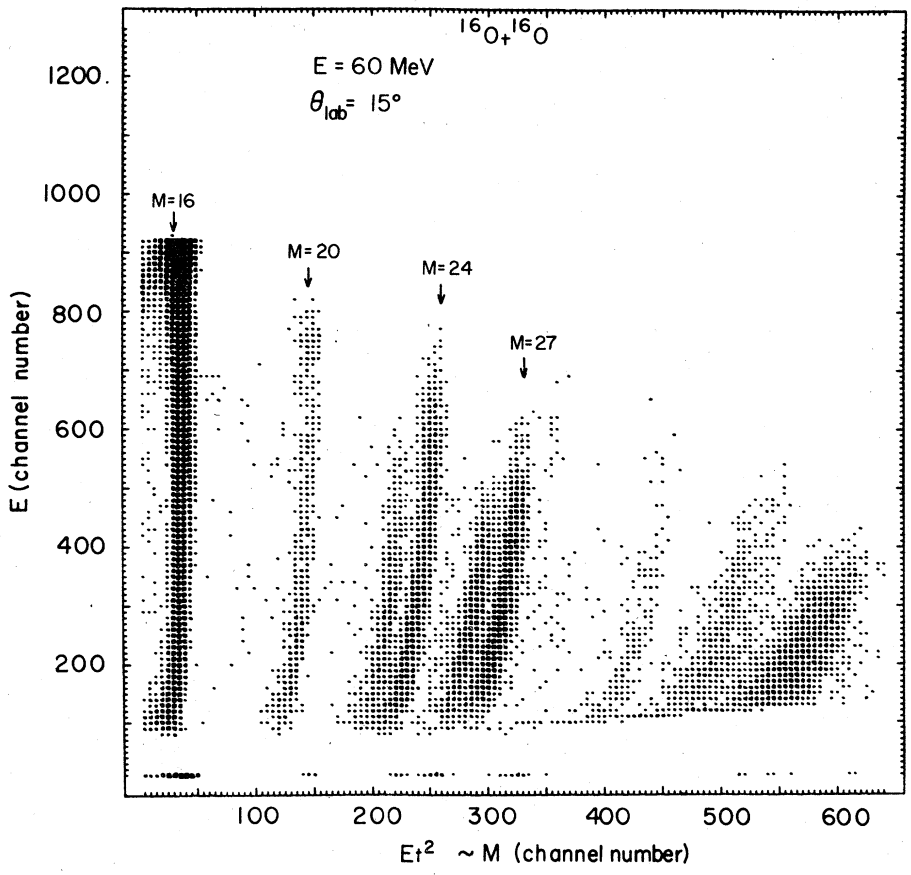

FIG. 2. A typical E vs M display for $^{16}O+^{16}O$ taken at $E_{lab}=60$ MeV and $\theta_{lab}=15°$.

yield. It should be pointed out that the ^{20}Ne represents a very small fraction of the fusion cross section. It increases with bombarding energy and reaches a value of only 10% at 66 MeV.

Two monitor detectors were placed symmetrically with respect to the beam direction at angles of ± 15°. The fusion yield N_F was normalized relatively to the sum of $^{16}O+^{16}O$ elastic scattering yield in the two counters. This procedure minimizes the effect of possible shifts of the beam direction during the measurements and is very essential for an accurate determination of the cross sections. The absolute differential fusion cross section is then given by

$$\frac{d\sigma_F}{d\Omega} = 2N_F \left(\frac{d\sigma}{d\Omega}\right)_{ela} \frac{1}{N_+ a_+ + N_- a_-},$$

where N_+ (N_-) is the elastic scattering yield in the right (left) monitor and a_+ (a_-) is the solid angle ratio between the telescope and the right (left) monitor. The elastic scattering cross section $(d\sigma/d\Omega_{ela})$ was measured from 17 to 66 MeV in an independent measurement using the same geometry. The target consisted of SiO_2 with a thin Au layer. In these measurements the telescope was set at 15° and the yields in the telescope and the monitors served to determine the ratios a_+ and a_-. The scattering of ^{16}O on Au obeys the Rutherford scattering law in this energy range and the amount of ^{16}O relative to Au in the target was obtained assuming pure Mott scattering in the energy range 17–20 MeV. In order to avoid any possible interference with the inelastic scattering on ^{28}Si, the measurements were repeated with a WO_3 target at several energies above 40 MeV. Very good agreement was obtained between the two target measurements. The results of the elastic scattering excitation function are shown in Fig. 3.

Complete angular distributions of the fusion cross section consisting of 8–10 points in the angular range $\theta_{lab}=4°-30°$ were measured at 3 MeV intervals from 27 to 66 MeV. The fusion yield could not be measured at angles below 4° because of the high counting rate of the elastic scattering. Figure 4 shows total angular distributions taken at 32 and 42 MeV with the ΔE-E telescope and at 57 MeV with the TOF technique. The differential cross sections are forward peaked,

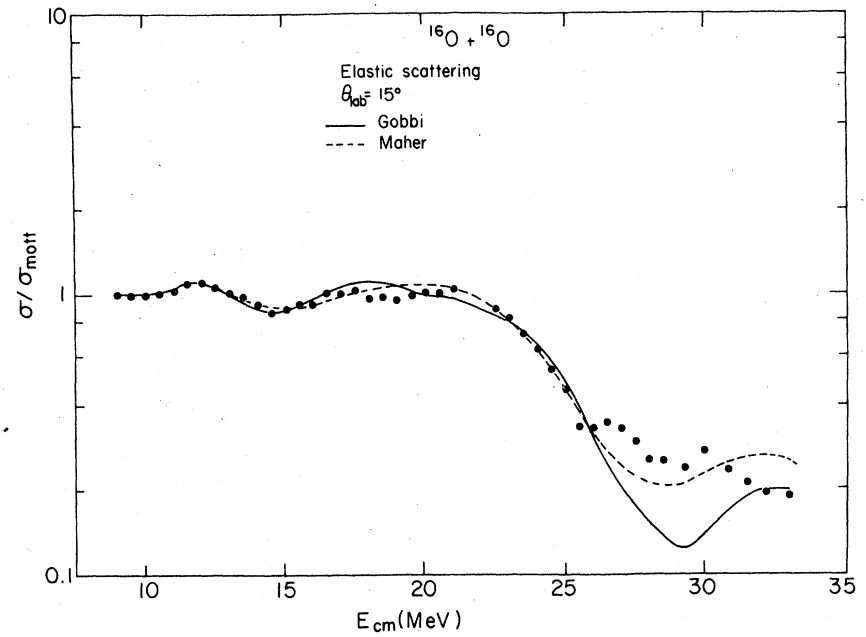

FIG. 3. Excitation function of $^{16}O + ^{16}O$ elastic scattering measured at $\theta_{lab} = 15°$. The experimental errors are smaller than the size of the points. The solid and dashed lines are optical model calculations using the Gobbi potential (Ref. 17) ($V_0 = 17$ MeV, $r_{0R} = 1.35$fm, $a_R = 0.49$ fm, $W_0 = 0.8 + 0.2\ E_{c.m.}$MeV, $r_{0I} = 1.27$ fm, $a_I = 0.15$ fm) and the Maher potential (Ref. 18) ($V_0 = 17$ MeV, $r_{0R} = r_{0I} = 1.35$ fm, $a_R = a_I = 0.49$ fm, $W_0 = 0.4 \pm 0.1\ E_{c.m.}$MeV), respectively.

falling approximately by a factor of 100 between 4° and 30°. It is seen that the shape of the angular distribution changes very little with incident energy. We took advantage of this well known fact and for the intermediate energies only three to five angles were measured. The statistical accuracy of the fusion yield was better than 3% for the angles which contribute most to the cross sections, i.e., 4°–15°.

Figure 5 displays the angular distributions of residual masses measured at 45 and 54 MeV with the TOF technique. The lines through the experimental points have been drawn to guide the eye. The shape of the angular distributions is governed mainly by the kinematics of the evaporation process. As more particles are evaporated by the compound nucleus, more lateral momentum is transferred to the residual nucleus and the angular distribution extends towards larger angles. The energy spectra are also determined to a large extent by kinematic considerations. These well known features will not be further discussed in this work.

The fusion cross section at a given energy was obtained by integration of the angular distribution. The extrapolation into the angular region not measured (0°–4°) was performed by fitting the angular distribution in the range 0°–7° with an expression of the form

$$\frac{d\sigma}{d\Omega} = a + b\theta^2 .$$

This form assures a zero slope of the differential cross section at 0°. The contribution of the angular range 0°–4° to the total fusion cross section was ≈ 13% in agreement with statistical model calculations (see Sec. 3.2). At bombarding energies where only a few angles were measured, the fusion cross section was deduced assuming the same shape of the angular distribution as for the closest energy for which a complete angular range was measured.

The results of the $^{16}O + ^{16}O$ fusion excitation function are presented in Fig. 6 as a function of the center-of-mass energy. An error of 5% has been assigned to each experimental point. This represents an upper limit of the total accuracy calculated from the individual factors discussed above (statistical accuracy, Ni correction, normalization procedure). The error of 5% is also consistent with the spread of experimental values for the same points measured in different runs and with different experimental methods.

III. ANALYSIS AND DISCUSSION

A. Total fusion excitation function

The total fusion cross section shows oscillations as a function of incident energy with an almost reg-

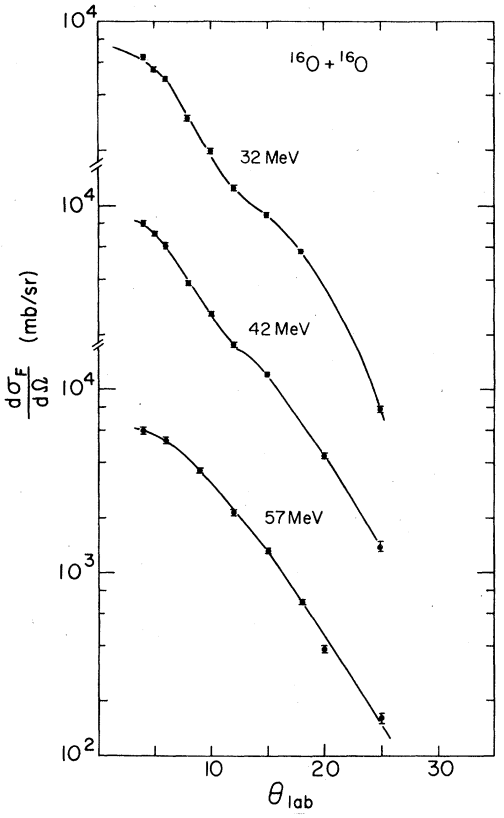

FIG. 4. Total angular distributions of evaporation residues from the fusion of $^{16}O + ^{16}O$. The lines have been drawn through the points to guide the eye.

ular spacing of about 3–4 MeV in the center-of-mass system (see Fig. 6). The structure becomes more pronounced with increasing energy and a particularly strong dip is observed at $E_{c.m.} = 28$ MeV. A similar structure has been recently observed in other measurements of the $^{16}O + ^{16}O$ fusion cross section using the γ-ray technique.[7,13] A comparison of the experimental results is presented in Sec. III C. The solid and dashed lines in Fig. 6 represent the total reaction cross section calculated with an optical model code using the parameters of Gobbi *et al.*[17] and of Maher *et al.*,[18] respectively. These two sets of parameters are characterized by a weak absorption at the nuclear surface (reflecting the availability of only very few direct channels) and were obtained from an extensive study of the $^{16}O + ^{16}O$ elastic scattering. The shape resonances produced in the reaction cross section by these surface-transparent potentials are in agreement both in location and width with the observed structure in σ_F. This was first pointed out by Kolata *et al.*[7] The magnitude of the structure in σ_F is not well reproduced by the shape resonances in σ_R at high incident energies. It should be mentioned that better agreement can be obtained by making small changes in the geometry of the imaginary potential. However, we chose not to change the optical parameters to force agreement between σ_F and σ_R. The important feature is the occurrence of the same resonant structure in the fusion and the total reaction cross sections. This gives strong support to the description[17–19] of the $^{16}O + ^{16}O$ interaction by a surface-transparent potential.

The reaction cross sections calculated with the Gobbi and the Maher potentials are in good agreement at low incident energies (see Fig. 6). At high energies the Maher potential gives higher values of σ_R as compared to the Gobbi potential. As expected, σ_F exhausts 90% or more of σ_R at energies below $E_{c.m.} = 20$ MeV. At higher energies, as more direct channels become available, σ_F decreases with respect to σ_R and accounts on the average for 75–80% of σ_R.

Figure 3 shows a comparison of the elastic scattering excitation function measured at 15° with optical model calculations using the Gobbi potential (solid line) and the Maher potential (dashed line). Good agreement is obtained with both sets up to $E_{c.m.} = 25$ MeV. At higher energies there are serious deviations particularly with the Gobbi potential.

B. Evaporation calculations

Angular distributions and relative production of residual nuclei were calculated using the code JULIAN developed by Hillman and Eyal.[20] The code includes evaporation of n, p, α, and γ and takes explicitly into account the angular momentum of the compound nucleus and of the emitted particles. The code was modified so that the m-state population is followed in the decay chain, thus enabling the calculation of the angular distribution of the light particles without a s-wave approximation. The initial spin distribution σ_J of the compound nucleus was calculated as in Ref. 14. The procedure is briefly outlined here. σ_J is given by

$$\sigma_J = \pi \lambda^2 (2J+1) T_J .$$

The coefficients T_J were calculated using the relation $T_J = [1 + \exp(l - l_c)/\Delta]^{-1}$. The l-diffuseness Δ was obtained by fitting a similar function to the transmission coefficients calculated with an optical model code using the Gobbi potential.[17] The value of l_c was determined by satisfying the condition that $\sum \sigma_J$ equals the experimental fusion cross section. This procedure removes the highest partial waves which presumably do not contribute to the fusion process. For more details on the input parameters for the code see Ref. 14.

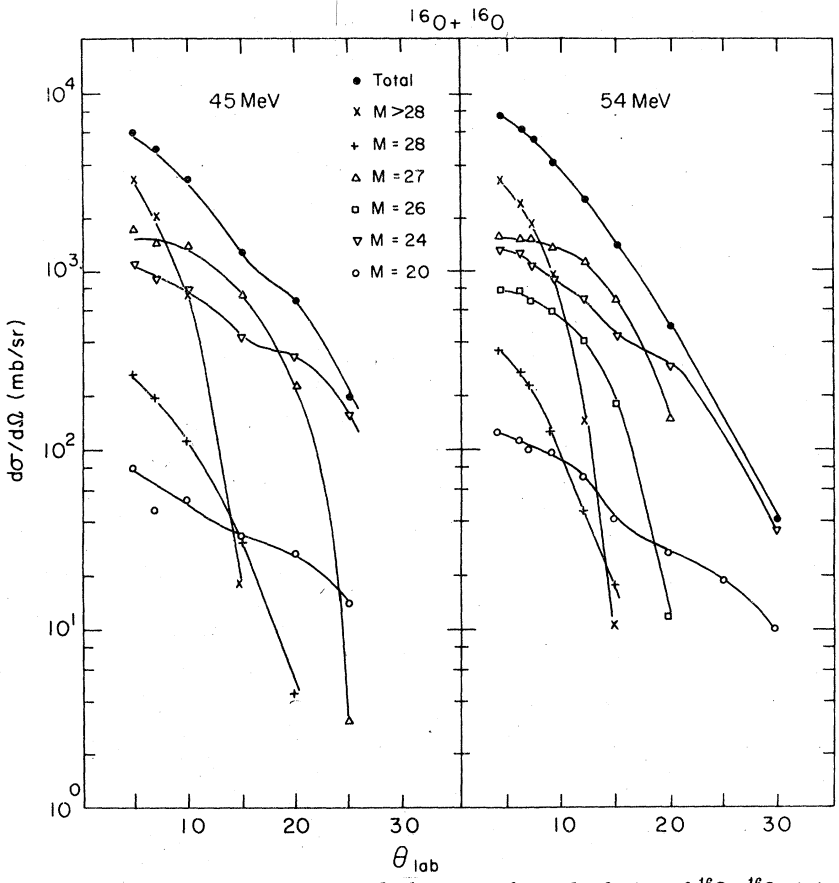

FIG. 5. Angular distributions of the dominant residual masses from the fusion of $^{16}O+^{16}O$ at 45 and 54 MeV.

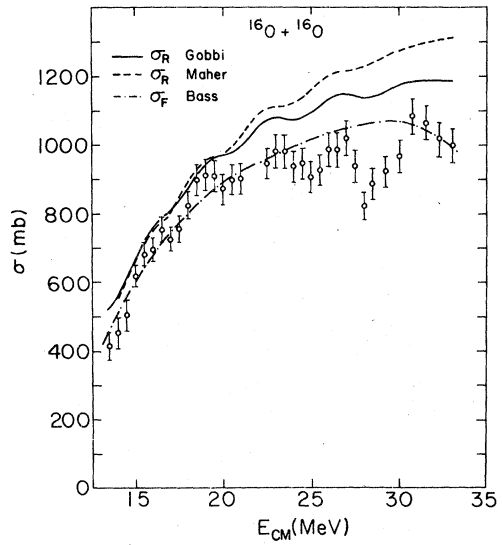

FIG. 6. Total fusion cross section σ_F (points) of $^{16}O+^{16}O$ as a function of the center-of-mass energy. The solid and dashed lines represent the total reaction cross section extracted from optical model calculations using the Gobbi potential (Ref. 17) and the Maher potential (Ref. 18), respectively. The dot-dashed line is a calculation of σ_F based on the Bass model (Ref. 27).

The level densities were generated using the method of Hillman and Grover[21] (HG) and the expression of Gilbert and Cameron[22] (GC). For the last one, the spherical nuclei value was taken for the level density parameter a.[22] Discrete low-lying levels and their spins were taken from the experimental data compiled in Ref. 23.

Calculated angular distributions are presented in Fig. 7 with experimental data at 32, 42, and 54 MeV. The solid and dashed lines were obtained using the HG and GC level densities, respectively. Reasonably good agreement is observed. In general the calculations with the HG level density overestimate the cross section at small angles and underestimate it at large angles. The opposite trend occurs with the GC level density. Note that this feature is nearly independent of the bombarding energy. It is interesting to point out that calculations performed under the assumption that the light particles are emitted isotropically in the center-of-mass system gave similar results. As expected, the yield is slightly decreased at forward angles and correspondingly increased at larger angles.

Figure 8 compares the mass distributions mea-

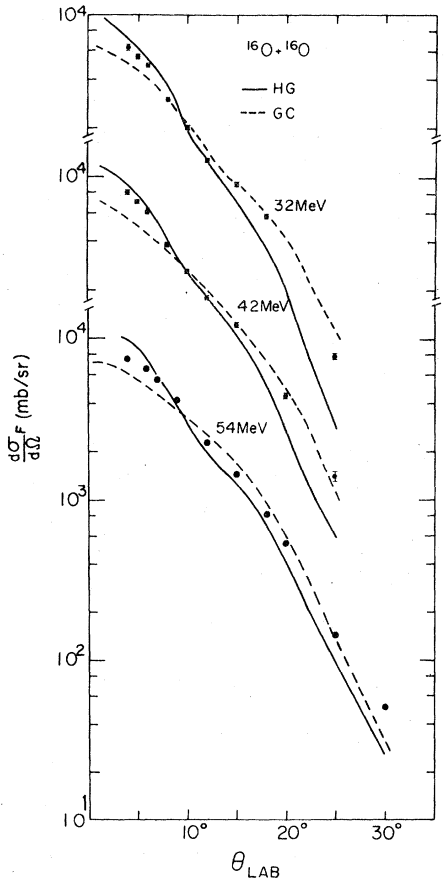

FIG. 7. Experimental fusion angular distributions at incident energies of 32, 42, and 54 MeV. The solid and dashed lines are statistical model calculations using the Hillman-Grover (Ref. 21) (HG) and Gilbert-Cameron (Ref. 22) (GC) level densities, respectively.

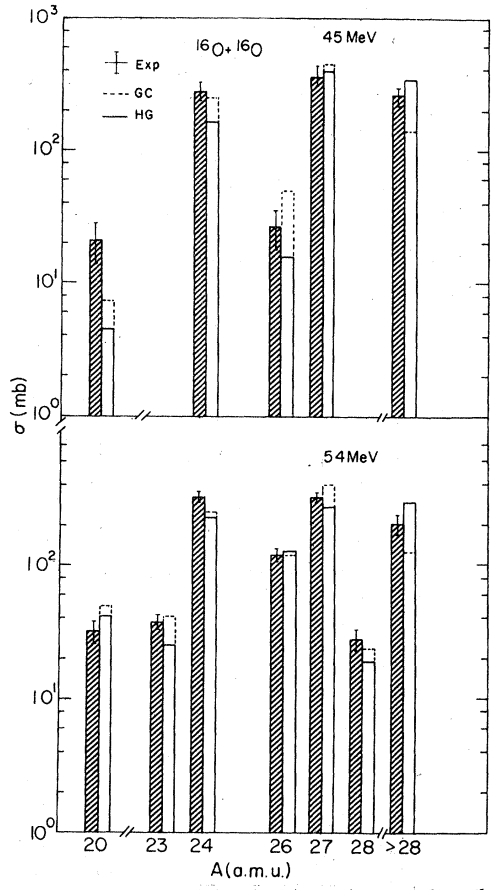

FIG. 8. Experimental (dashed boxes) mass distributions from the fusion of $^{16}O+^{16}O$ at 45 and 54 MeV, compared to statistical model calculations using the HG (solid line) and GC (dashed line) level densities.

sured at 45 and 54 MeV using the TOF technique with the evaporation calculations. Experimentally, the most abundant products are $A=24$ and $A=27$. They are obtained by emission of 2α and αp, respectively, since on the average the compound nucleus evaporates two or three particles. They account for more than 50% of the fusion cross section at both energies in agreement with the calculations. The decay products involving α-particle emission are slightly overestimated (underestimated) by the calculations using the GC (HG) level density. This is reflected in the total angular distribution by the overestimation (underestimation) of the cross section at large angles.

As it appears from Figs. 7 and 8, the main features of the data are well described by the evaporation model. Since the different steps in the decay process are treated exactly, it seems that the observed small discrepancies can be mainly attributed to the level density which is the least known factor entering the calculations. (Other factors such as the optical potentials parameters for light particles have only a very small effect on the results.) Figures 7 and 8 illustrate the sensitivity of the results on the level density. The parameters defining the GC level density have an appreciable influence on the calculations, as shown in Ref. 24. Note also that possible contributions of nonstatistical effects cannot *a priori* be ruled out, particularly at high energies. However, as mentioned above, the data do not show systematic deviations from the statistical calculations as a function of bombarding energy.

C. Comparison with other experiments

Excitation functions of the $^{16}O+^{16}O$ fusion cross section have recently been measured by Kolata *et al.*[7] ($E_{lab}=25$–61 MeV) and by Cheng *et al.*[13] ($E_{lab}=18$–60 MeV) using the γ-ray technique. Figure 9 compares the results of the present work with those obtained in Refs. 7 and 13. Such a comparison is interesting since it might give in-

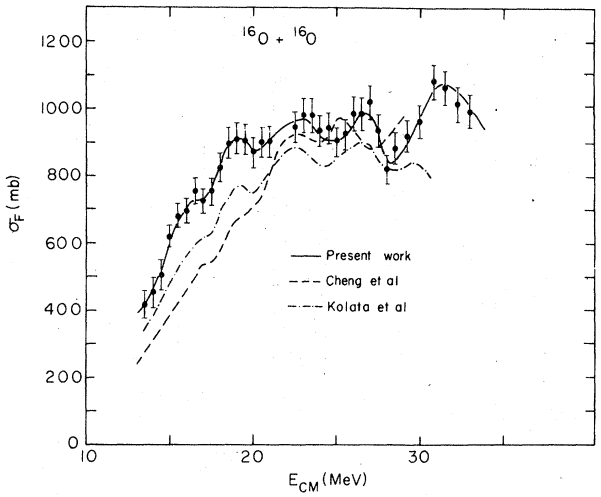

FIG. 9. Fusion cross sections measured in the present work (points). The solid line has been drawn smoothly through the experimental points. The dashed and the dot-dashed lines are smooth curves drawn through the data of Ref. 13 and of Ref. 7, respectively.

formation about the importance of direct population of ground states and high energy γ transitions to ground states (from levels above 4 MeV in Ref. 13 and above 6 MeV in Ref. 7) which are not taken into account with the γ-ray technique. This missing cross section can be particularly important at low energies as pointed out in Refs. 14 and 25 for the $^{16}O + ^{27}Al$ system. First we note that the cross sections reported in the two γ-ray works differ one from the other by almost 100 mb. The cross sections of Ref. 7 are higher at lower energies and lower at high energies than those of Ref. 13. On the average, both cross sections are lower than those reported here. The deviations are of the order of 20–30% at low energies and smaller (5–10%) at high energies. In order to investigate whether these discrepancies can be accounted for by the missing cross section in the γ-ray studies, the ground state population was calculated using the statistical model. The results are given in Table I. They clearly indicate that the ground state population is an important mode of decay and cannot be neglected. The calculated unobserved flux in the γ-ray work is comparable in magnitude to the deviations shown in Fig. 9 although it decreases too slowly with increasing incident energy. Table I also shows that the missing cross section is distributed over different residual nuclei. The contribution of high γ-ray transitions to ground states is relatively small (about 5%) for $E_\gamma > 4$ MeV, and practically negligible (1–2%) for $E_\gamma > 6$ MeV.

It is interesting to note that in spite of the missing cross section, the structure observed in Ref. 7 is in good agreement with the present work. The location, width, and magnitude of the resonances agree in both works up to $E_{c.m.} = 29$ MeV. At higher energies our data show a strong maximum of σ_F while the data of Ref. 7 indicate a constant or even decreasing cross section. The structure observed in the work of the Stanford group is also in good agreement but only up to $E_{c.m.} = 25$ MeV.

The $^{16}O + ^{16}O$ fusion cross section has also been measured by Weidinger *et al.*[24] at $E_{lab} = 60$ MeV using the TOF technique. They report a cross section of 1000± 150 mb in agreement with the value of 965± 50 mb in the present work.

D. Average energy dependence of σ_F

Figure 10 shows the fusion cross section as a function of $1/E_{c.m.}$. The solid line has been drawn through the experimental points to guide the eye. The barrier and critical parameters were obtained using the phenomenological model of Glas and Mosel.[4] In this model a parabolic barrier approximation is used with l-independent curvature $\hbar\omega$. The fusion cross section is given by

$$\sigma_F = \frac{\hbar\omega R_B^2}{2E_{c.m.}} \ln \frac{1+\exp[2\pi(E_{c.m.} - V_B)/\hbar\omega]}{1+\exp\{2\pi[E_{c.m.} - V_B - (E_{c.m.} - V_C)R_C^2/R_B^2]/\hbar\omega\}}.$$

TABLE I. Relative ground state populations (via particle decay or γ transitions from levels above 4 MeV) $\sigma_{g.s.}/\sigma_F$ (%) for different incident energies.

E_{lab} (MeV)	$\sigma_{g.s.}/\sigma_F$ (%) ^{30}P	^{30}Si	^{27}Al	^{26}Al	^{24}Mg	^{23}Na	^{20}Ne	$\sum\sigma_{g.s.}/\sigma_F$ (%)
28	8.2	4.4	4.2	•••	4.6	•••	•••	22
32	5.4	2.1	5.9	•••	5.0	•••	•••	19
38	4.0	0.8	7.1	•••	5.6	•••	•••	18
54	0.6	0.2	4.3	1.3	2.4	4.2	3.8	17
60	0.1	0.1	2.3	1.1	1.6	4.9	5.4	16

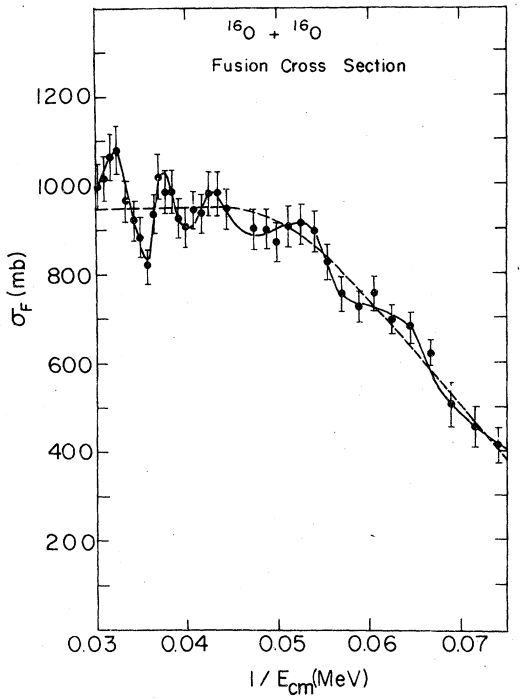

FIG. 10. Total fusion cross section vs $1/E_{c.m.}$. The solid line is a smooth curve drawn through the experimental points. The dashed line is a fit to σ_F based on the Glas and Mosel model (Ref. 4).

The dashed line in Fig. 10 is a three-parameter fit (R_B, V_B, and R_C) to σ_F. The value of V_C could not be accurately fitted because of the pronounced structure of the fusion cross section at high energies. V_C was therefore kept equal to zero as suggested by the average behavior of the high energy data (in this energy region the fusion cross section is given by $\sigma_F = \pi R_C^2 (1 - V_C/E_{c.m.})^4$. The parameter $\hbar\omega$ characterizing the behavior of the fusion cross section at very low energy near and below the Coulomb barrier was also kept constant $\hbar\omega = 3$ MeV. Changing this parameter by 1 or 2 MeV produced only minor changes in the other parameters. The parameters used in the fit are listed in Table II. The average behavior of the fusion exictation function shows the familiar picture of two straight lines connected by a smooth bend. The bend occurs at an energy $E_{c.m.} \approx 19.5$ MeV. This is in disagreement with the analysis of Ref. 13 which gives the bend at $E_{c.m.} = 27$ MeV. It should be mentioned that for other systems in this mass region the bend occurs at energies $E_{c.m.} = 18$–20 MeV, e.g., for the system $^{14}N + ^{12}C$, it occurs at 18.5 MeV [9,10] and for $^{18}O + ^{12}C$ at 20 MeV.[6] The parameters obtained in Ref. 13 are also listed in Table II. It is seen that the V_B values are in good agreement, whereas the r_{0B} values differ by ~ 14%. This is due to the discrepancies in the absolute cross sections as discussed in the previous section. The critical parameters could not be obtained in Ref. 13 due to the lack of high energy data beyond the apparent bend at 27 MeV.

For the sake of comparison the parameters obtained from the neighboring systems $^{16}O + ^{12}C$, $^{14}N + ^{12}C$, and $^{18}O + ^{12}C$ are also listed in Table II. The parameters from these systems are very similar to those obtained from $^{16}O + ^{16}O$. In particular there is no clear manifestation of shell effects in the fusion cross section, at least not in the way predicted by Glas and Mosel,[4,12] i.e., through a lower r_{0C} value as compared to neighboring nonclosed shell systems. The critical radius and also the barrier radius for the $^{16}O + ^{16}O$ system do not show deviations with respect to the average values obtained from the other systems.

Also, the experimental value of the $^{16}O + ^{16}O$ fusion cross section in the bend region σ_F^{max} is comparable to the average value[11] ($\sigma_F^{max} \approx 900$–$1000$ mb) obtained in the fusion of $1p$-shell nuclei. Assuming a zero slope of σ_F vs $1/E_{c.m.}$ at high energies (see Fig. 10), a value of $\sigma_F^{max} \approx 950$ mb is obtained for the $^{16}O + ^{16}O$ system. The $^{15}N + ^{12}C$ system remains an exceptional case among the $1p$-shell nuclei with its anomalously high value of $\sigma_F^{max} \approx 1200$ mb.[9]

From the above discussion we conclude that the average trend (i.e., neglecting the oscillations) of the fusion of $^{16}O + ^{16}O$ behaves similarly to other systems in this mass region. The effective poten-

TABLE II. Barrier and critical parameters deduced from the fusion cross section of various neighboring systems. The radius parameter r_0 is obtained from $R = r_0 (A_1^{1/3} + A_2^{1/3})$.

System	r_{0B} (fm)	V_B (MeV)	r_{0C} (fm)	V_C (MeV)	Ref.
$^{16}O + ^{16}O$	1.63 ± 0.22	10.9 ± 1.1	1.09 ± 0.3	0	Present work
$^{16}O + ^{16}O$	1.46	11.5	...	...	13
$^{14}N + ^{12}C$	1.54	7.2	1.13	−2.9	9
$^{14}N + ^{12}C$	1.50	6.7	1.08	−2.0	10
$^{16}O + ^{12}C$	1.57 ± 0.03	7.69 ± 0.10	0.93 ± 0.03	−10	6
$^{18}O + ^{12}C$	1.60 ± 0.02	7.51 ± 0.05	1.04 ± 0.02	−10	6

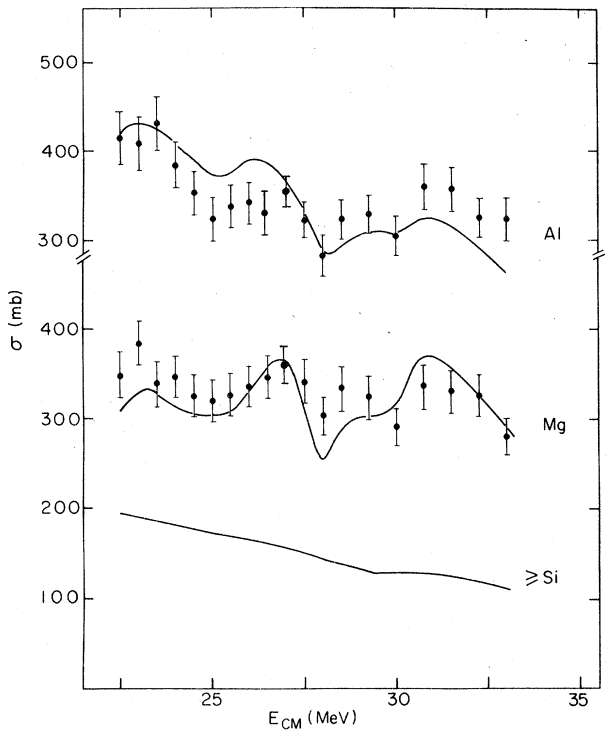

FIG. 11. Partial fusion excitation functions for different elements. The solid lines are statistical model calculations based on the code JULIAN (Ref. 20) using the GC level densities.

tial required to reproduce these data follows the systematics of neighboring systems. The same conclusion is drawn from an analysis of the $^{16}O + ^{16}O$ fusion data using the Bass model.[26,27] The dot-dashed line in Fig. 6 is a calculation of the fusion cross section following Ref. 27. These calculations use an effective nucleus-nucleus potential derived from a fit to fusion cross sections of a large set of different colliding systems (including also high-mass systems). It is seen that the empirical potential reproduces the average trend of the $^{16}O + ^{16}O$ fusion data, although it tends to overestimate the cross section at high energies.

E. Excitation function σ_Z of residual elements

Figure 11 shows experimental partial fusion cross sections together with the theoretical predictions of the code JULIAN. For Al and Mg the calculations show oscillations which are in agreement with those observed in the total fusion cross section (see Fig. 6). Although the experimental errors are larger than for σ_F (since part of the yield is below the Bragg maximum and the statistics are poorer) a similar oscillatory pattern is apparent in the data. The experimental partial fusion cross section for Si and P could not be extracted from the ΔE-E data. For these elements only the calculations are presented showing a smooth behavior of the partial fusion cross section in agreement with the results of Kolata *et al.*[7] The residual elements Al and Mg are mainly produced by the decay of high spin states in the compound nucleus. This is demonstrated in the lower part of Fig. 12 which shows the relative population of residual nuclei as a function of the spin J of the compound nucleus at an incident energy of 63 MeV. The upper part of the figure gives the initial spin distribution of the compound nucleus. The higher spin states decay mainly into ^{27}Al (i.e., αp emission) and ^{24}Mg (2α), i.e., through α-particle emission which can remove a large amount of angular momentum. In the $^{16}O + ^{12}C$

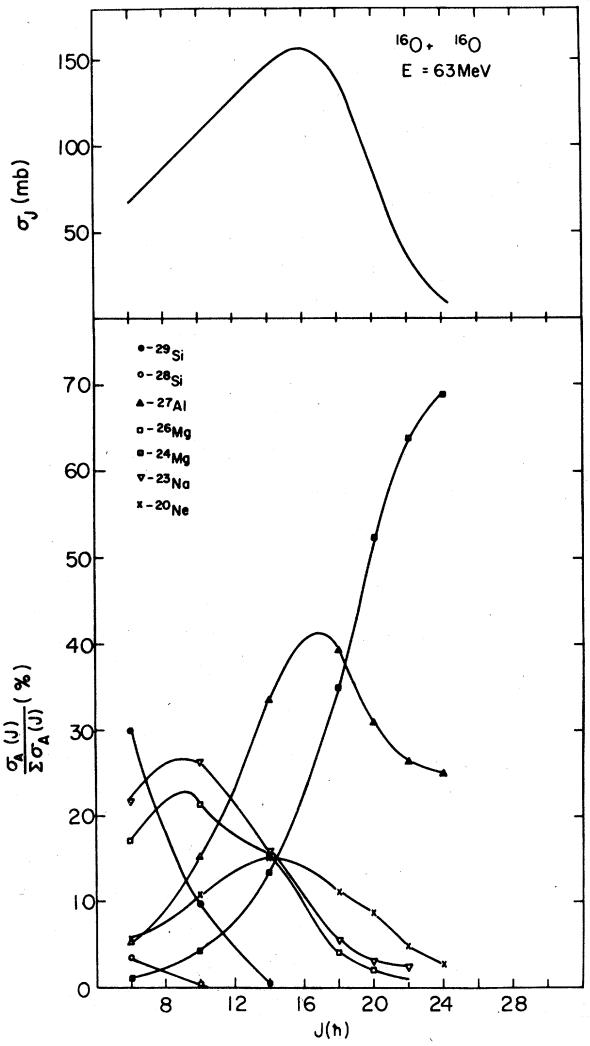

FIG. 12. Upper part: calculated spin population of the compound nucleus at $E_{lab} = 63$ MeV. Lower part: calculated relative population of residual nuclei as a function of the spin J of the compound nucleus.

system it was also shown that oscillations in σ_F are associated with channels involving α-particle emission.[28] The channels involving the decay of three particles such as ^{29}Si ($2pn$), ^{26}Mg ($2p\alpha$), ^{23}Na ($p2\alpha$), and ^{20}Ne (3α) come mainly from low spin values of the compound nucleus. It seems, therefore, that the oscillations in σ_F are mainly present in the residual nuclei ^{24}Mg and ^{27}Al and are associated with the high partial waves (as expected for shape resonances).

IV. SUMMARY

Evaporation residues produced in the fusion of ^{16}O + ^{16}O have been measured in the energy range E_{lab} = 27–66 MeV using the ΔE-E or the time-of-flight techniques. The total fusion excitation function shows oscillations with an almost regular spacing of 3–4 MeV in the c.m. system. These oscillations agree in location and width but not in amplitude with the resonances produced in the total reaction cross section by surface transparent potentials which fit the ^{16}O + ^{16}O elastic scattering.[17,18]

The mass and angular distributions are well reproduced by statistical evaporation calculations which take angular momentum into account explicitly.[20] These calculations, together with the measured partial fusion cross sections for production of Mg and Al, indicate that the oscillations in σ_F are mainly produced by the peripheral partial waves populating the compound nucleus.

Our results were compared with those obtained in other experiments using the γ-ray technique.[7,13] The agreement is generally good for the structure observed in σ_F. However, there are large deviations in the absolute cross section, the γ-ray values being systematically lower than ours. Evaporation calculations indicate that these discrepancies can be accounted for by direct decay into ground states which are not taken into account in the γ-ray measurements.

The average energy behavior of the fusion excitation function has been analyzed in the framework of the Glas and Mosel[4] and the Bass[27] models. Both analyses indicate that the fusion of ^{16}O + ^{16}O follows the macroscopic systematics of neighboring systems with the exception of ^{15}N + ^{12}C. In particular, no evidence of shell effects (through a reduction of the critical distance R_C as predicted by Glas and Mosel[12]) is found in the fusion of ^{16}O + ^{16}O.

We are pleased to acknowledge Dr. Z. Fraenkel and Dr. R. G. Stokstad for a careful reading of the manuscript, and Dr. R. Bass for calculating σ_F according to his model.

---

*Present address: Israel Atomic Energy Commission, Soreq Nuclear Research Center, Yavne, Israel.
†Supported by the Minerva Foundation. Permanent address, Physialisches Institut, Universitat Heidelberg.
‡Present address: Centre de Researches Nucleaires, Strasbourg, France.

[1]See, e.g., Proceedings of the European Conference on Nuclear Physics with Heavy Ions, Caen, 1976, in J. Phys. C5, 1976.
[2]H. H. Gutbrod, W. G. Winn, and M. Blann, Nucl. Phys. A213, 267 (1973); W. Scobel, H. H. Gutbrod, M. Blann, and M. Mignerey, Phys. Rev. C 14, 1808 (1976).
[3]M. Lefort, Rep. Prog. Phys. 39, 129 (1976), and references therein.
[4]D. Glas and U. Mosel, Nucl. Phys. A237, 429 (1975).
[5]P. Sperr, S. Vigdor, Y. Eisen, W. Henning, D. G. Kovar, T. R. Ophel, and B. Zeidman, Phys. Rev. Lett. 36, 405 (1976).
[6]P. Sperr, T. H. Braid, Y. Eisen, D. G. Kovar, F. W. Prosser Jr., J. P. Schiffer, S. L. Tabor, and S. Vigdor, Phys. Rev. Lett. 37, 321 (1976).
[7]J. J. Kolata, R. C. Fuller, R. M. Freeman, F. Haas, B. Hensch, and A. Gallmann, Phys. Rev. C 16, 891 (1977).
[8]Oscillations in σ_F have also been observed at very low energies for the systems ^{12}C + ^{12}C and ^{12}C + ^{16}O, see, e.g., R. G. Stokstad, Z. E. Zwitkowski, R. A. Dayras, and R. M. Wieland, Phys. Rev. Lett. 37, 888 (1976), and references therein.
[9]S. Harar, in Proceedings of the International Conference on Resonances in Heavy Ion Reactions, Hvar, 1977 (unpublished).
[10]R. G. Stokstad, T. Gomez del Campo, J. A. Biggerstaff, A. H. Snell, and P. H. Stelson, Phys. Rev. Lett. 36, 1529 (1976).
[11]J. P. Schiffer, in Proceedings of the International Conference on Nuclear Structure, Tokyo, 1977, edited by T. Marumori, [J. Phys. Soc. Jpn. Suppl. 44, 9 (1978)].
[12]D. Glas and U. Mosel, Phys. Lett. 49B, 301 (1974).
[13]V. K. C. Cheng, A. Little, H. C. Yuen, S. M. Lazarus, and S. S. Hanna, report, 1977 (unpublished).
[14]Y. Eisen, I. Tserruya, Y. Eyal, Z. Fraenkel, and M. Hillman, Nucl. Phys. A291, 459 (1977).
[15]M. M. Fowler and R. C. Jared, Nucl. Instrum. Methods 124, 341 (1975).
[16]C. K. Gelbke, K. D. Hildenbrand, and R. Bock, Nucl. Instrum. Methods 95, 397 (1971).
[17]A. Gobbi, R. Wieland, L. Chua, D. Shapira, and D. A. Bromley, Phys. Rev. C 7, 30 (1973).
[18]J. V. Maher, M. W. Sachs, R. H. Siemssen, A. Weidinger, and D. A. Bromley, Phys. Rev. 188, 1665 (1969).
[19]P. P. Singh, D. A. Sink, P. Schwandt, R. E. Malmin, and R. H. Siemssen, Phys. Rev. Lett. 28, 1714 (1972).
[20]M. Hillman and Y. Eyal (unpublished). See also Ref. 9, p. 109.
[21]M. Hillman and J. R. Grover, Phys. Rev. 185, 1303

(1969).
[22]A. Gilbert and A. G. W. Cameron, Can. J. Phys. 43, 1446 (1965).
[23]P. M. Endt and C. van der Leun, Nucl. Phys. A214, 1 (1973).
[24]A. Weidinger, F. Busch, G. Gaul, W. Trautmann, and W. Zipper, Nucl. Phys. A263, 511 (1976).
[25]J. Dauk, K. P. Lieb, and A. M. Kleinfeld, Nucl. Phys. A241, 170 (1975).
[26]R. Bass, Phys. Lett. 47B, 139 (1973); Nucl. Phys. A231, 45 (1974).
[27]R. Bass, Phys. Rev. Lett. 39, 265 (1977).
[28]S. L. Tabor, Y. Eisen, D. G. Kovar, and Z. Vager, Phys. Rev. C 16, 673 (1977).